Geotextiles and Geomembranes 54 (2026) 1285–1298

Contents lists available at ScienceDirect

Geotextiles and Geomembranes

journal homepage: www.elsevier.com/locate/geotexmem

Regular Paper

On the assessment of the wettability and wickability of nonwoven wicking geotextiles

Ali Pezeshki [a,*], Mohamed A. Meguid [a], Sam Bhat [b]

[a] Department of Civil Engineering, McGill University, 817 Sherbrooke St. W., Montreal, QC, H2A 0C3, Canada
[b] Chief Technical Officer, Titan Environmental Containment Ltd, Canada

ARTICLE INFO

Keywords:
Nonwoven wicking geotextile
Capillary flow
Wettability
Wicking rate
Contact angle
Mechanical clogging

ABSTRACT

The growing application of nonwoven wicking geotextiles for capillary water drainage in transportation embankments highlights the need to better understand the hydraulic mechanisms governing their field performance efficiency. Accordingly, this study investigated wettability and wickability in nonwoven geotextiles, emphasizing pore structure as the critical link between these two distinct phenomena. Experimental characterization was conducted through contact angle (CA) measurements using water, glycerin, and mineral oil droplets, alongside horizontal radial wicking tests with an infinite water source. The latter test provided a more representative assessment of material-scale wicking behavior than CA measurements. Two nonwoven wicking geotextiles (WGv1 and WGv2) and one nonwicking control (NG) were evaluated. The use of a wide range of probe liquids and nonwoven geotextiles enabled the assessment of diverse wetting interactions and the measurement of wicking rates for various liquid–geotextile combinations. Notably, enhanced wettability did not always result in higher wicking rates. WGv1, with its more open and porous structure, consistently exhibited a greater wicking rate than WGv2, which featured a denser configuration. Additional tests on a wicking sample impregnated with fine glass beads showed lower gravimetric liquid retention and diminished water wicking performance, highlighting the importance of evaluating soil–geotextile interaction.

1. Introduction

Geotextiles are multifunctional geosynthetic materials widely employed in transportation embankments for separation, reinforcement, filtration, barrier, and drainage applications (Bouazza et al., 2013; Han, 2015; Koerner, 2012). With the advent of wicking fibers, the drainage function of geotextiles has expanded to encompass drainage in both saturated and partially saturated soil conditions. The hydrophilic properties and interconnected pore structure of wicking geotextiles allow them to absorb moisture from adjacent soil deposits and transport it to exposed edges for evaporation and drainage. The enhanced wetting regime between the hydrophilic fibers and water creates a higher capillary suction within the geotextile, allowing moisture to be drawn from the surrounding soil into the fibrous pore network. The absorbed moisture is subsequently transported through the interconnected pore structure by capillary pressure gradients sustained by evaporation or free drainage at the exposed edges. This sustained moisture reduction significantly enhances embankment stability and mitigates pavement distress. Guo et al. (2026) reported that wicking geotextiles delayed soil saturation during rainfall while enhancing post-rainfall moisture removal in silty embankments. Moisture control in partially saturated conditions is equally as critical as drainage under saturated conditions for transportation infrastructure (Azevedo and Zornberg, 2013; Lekarp et al., 2000; Lin et al., 2016, 2018; Uzan, 2004).

Laboratory studies have demonstrated that the performance of granular materials in transportation embankments is sensitive to moisture content. Li et al. (2011) indicated that the resilient modulus of a high-quality base granular material decreased by approximately half when the moisture content increased from 3.5% to 6.0%. More recently, Ma et al. (2024) used numerical modeling to show a 30% increase in resilient modulus following a 5% moisture reduction achieved through the use of wicking fibers. Similarly, Lin et al. (2018) reported a 480 MPa increase in resilient modulus after a 3% moisture reduction in an aggregate base. These findings highlighted the importance of moisture management in partially saturated soils, where even minor changes in water content can cause significant mechanical performance shifts.

Moisture accumulation also significantly influences the deformation of unbound granular materials. Liu et al. (2025a) reported an additional

* Corresponding author.
E-mail addresses: ali.pezeshkinajafabadi@mail.mcgill.ca (A. Pezeshki), mohamed.meguid@mcgill.ca (M.A. Meguid), sam.bhat@titanenviro.com (S. Bhat).

https://doi.org/10.1016/j.geotexmem.2026.07.006
Received 1 July 2025; Received in revised form 19 July 2026; Accepted 19 July 2026
Available online 28 July 2026
0266-1144/

128% increase in stiffness in a lab-scale unpaved embankment using a wicking geocomposite composed of a wicking geotextile and geogrid, compared to a similar system with a nonwicking geotextile. Haynes and Yoder (1963) found that total permanent axial strain increased by over 100% when saturation rose from 60% to 80%. In cold regions, freeze-thaw cycles further exacerbate pavement deterioration, leading to frost heave, thaw weakening, and reduced pavement ride quality (Sylvestre et al., 2019). Field investigations provided compelling evidence of the effectiveness of wicking geotextiles. Zhang et al. (2014) documented the use of wicking geotextile beneath an Alaskan pavement to mitigate the detrimental effects of frost boiling, while Galinmoghadam et al. (2022) reported approximately a 10% reduction in volumetric moisture content resulting from their application. Zornberg et al. (2017) also reported multiple field cases where wicking geotextiles mitigated pavement distress, longitudinal cracks, frost heave, and settlement.

Wicking geotextiles absorb moisture from adjacent partially saturated soils due to their high surface energy and transport the absorbed water along their in-plane direction. Moisture transport at the geotextile–soil interface is influenced by the wettability characteristics of materials. Rollin and Lombard (1988) described wettability as the hydraulic property controlling the water potential required for water to penetrate dry porous structures. Zornberg et al. (2010) further highlighted that enhanced wettability facilitates moisture transport by dissipating the capillary barrier between soil and wicking fibers and lowering the geotextile's resistance to wetting. Capillary liquid transport in porous media, known as wicking, occurs due to a suitable wetting regime and an interconnected pore structure. Thus, wicking can be considered a consequence of wetting, but it is strongly influenced by pore size, pore connectivity and geometry, and fiber orientation in nonwovens (Kissa, 1996; Van Der Meeren et al., 2002; Zhong, 2006).

In the context of this study, wettability refers to the affinity between the geotextile fiber surface and a liquid, which governs the initiation of wetting and is commonly characterized by the contact angle. Wettability is a prerequisite for wicking, which is the spontaneous transport of liquid through the interconnected pore network. Accordingly, wickability is defined as the ability of a nonwoven wicking geotextile to absorb and transport liquid by capillary action through its fibrous pore network. The wicking rate is the measured rate of liquid transport and serves as a quantitative measure of wickability. The imbibition rate describes the rate at which an individual liquid droplet is absorbed into the geotextile under transient wetting conditions. Also, the term absorption is used only in a general sense to describe liquid uptake.

To accurately assess the performance of wicking geotextiles, it is critical to differentiate clearly between wettability and wickability, as enhanced wettability alone does not necessarily ensure improved wickability or effective moisture management within embankments. This limitation is exemplified by situations where microscopic capillaries in woven geotextiles become obstructed or damaged (Lin et al., 2017) or where structural discontinuities in nonwoven fabrics flatten the liquid meniscus and impede flow, despite their high inherent wettability (Rengasamy, 2006). In such cases, the functionality of moisture redistribution in the embankment may be significantly compromised.

Zhong (2006) defined wetting as the replacement of a solid–air interface with a solid–liquid interface, whereas wicking refers to the self-driven movement of liquid through a porous network due to capillary action. Harnett and Mehta (1984) highlighted confusion in some wickability testing methods, attributing it primarily to the lack of distinction between wicking and wetting phenomena. Wickability in textile products has been evaluated using capillary rise tests by measuring the velocity of the advancing liquid front (Kim et al., 2022; Sharabaty et al., 2008; Stormont and Morris, 2000). Bouazza (2014) emphasized that both wettability and pore size are key factors influencing the final height of the liquid front in capillary rise tests.

Analysis of droplet spreading and imbibition on porous surfaces during the contact angle test constitutes a standard method for determining surface wettability and evaluating wicking dynamics. Zaman et al. (2022) investigated surface wettability in conventional nonwoven, woven, and wicking woven geotextiles using droplet contact angle tests. Their water droplet dissipation analyses on hydrophilic fibers indicated wickability and the strong wetting regime imposed by the deep-grooved nylon channels in wicking woven geotextiles. Liu et al. (2025b) also reported a high capacity of nonwoven wicking geotextiles to absorb water droplets during the contact angle test, indicating strong capillary forces between water and the fiber surfaces due to enhanced wettability.

Previous investigations of wicking geotextiles in transportation embankments generally focused on woven products that unidirectionally transport moisture under partially saturated conditions through hydrophilic, deep-grooved nylon yarns (Bai et al., 2024; Lin et al., 2022). Bouazza (2014) employed capillary rise tests to demonstrate increased hydrophilicity in chemically treated nonwoven needle-punched polyester geotextiles. More recently, surface treatments have been industrially applied to the filaments used in nonwoven geotextiles, introducing a durable hydrophilic regime to previously hydrophobic fibers. Nevertheless, the study of nonwoven wicking fibers in geotechnical engineering is still in its early stages, and research on their wettability and wickability remains limited (Jarjour et al., 2024; Liu et al., 2025a, 2025b).

Moisture transport in nonwoven products occurs through an interconnected fibrous pore network, making it essential to distinguish the roles of fiber wettability and pore structure in governing wickability. Consequently, this study investigates the contributions of wettability and pore structure to the wickability of nonwoven wicking geotextiles. Furthermore, because their fibrous pore structure is susceptible to alteration by particle impregnation, the influence of filtration-induced clogging on their wicking performance is also evaluated to provide insight into their long-term hydraulic behavior.

Additionally, it is worth mentioning that fluid transport terminology varies across disciplines. In soil mechanics, the rate of flow through porous media is commonly described by the hydraulic conductivity function across a range of suction levels and obtained either directly through experimentation or indirectly from the water retention curve (Brooks and Corey, 1965; Van Genuchten, 1980). The same framework can be applied to geotextiles when assessing their hydraulic response (Bouazza et al., 2006). Other material characterization methods for geotextiles, such as the bubble point test, offer valuable insights into the wettability and retention capacity of nonwoven materials (Aydilek et al., 2007). Elton and Hayes (2008) demonstrated that fiber wettability is a critical factor in porometry analysis conducted via capillary flow tests on nonwoven fibers (ASTM-D6767). Alternatively, textile research quantifies liquid transfer through the wicking rate, typically measured on initially dry samples supplied with either a finite or infinite liquid source.

The primary objective of this study is to clarify how intrinsic wettability and pore structure jointly influence the wicking rate in nonwoven geotextiles. To achieve this, contact angle measurements were performed using various test liquids on specimens with well-defined properties. The resulting data provided valuable insights into capillary flow in fibrous porous media, which is essential for the informed selection of wicking geotextiles during the design process. To address the limitations of droplet tests in representing moisture transport under field conditions, a horizontal radial wicking experiment with an infinite water reservoir was also conducted.

Additionally, the study investigated the influence of filtration-induced clogging on wicking performance under a controlled laboratory clogging condition. Particle migration during the filtration test was accelerated to produce a clogged state representative of the potential hydraulic consequences of particle impregnation within a practical laboratory timescale.

2. Materials

2.1. Geotextile samples and probe liquids

Three continuous filament needle-punched nonwoven geotextiles produced on the same manufacturing line were selected for comparative evaluation of wettability and wickability. These fabrics differ in the extent of coating treatment received and in their pore structure, while exhibiting nearly identical mechanical properties. The products comprise a white wicking geotextile (*WGv_1*), a grey wicking geotextile (*WGv_2*), and a white nonwicking reference geotextile (*NG*). The two wicking variants (WGv_1 and WGv_2) are manufactured from polyester filaments that receive a hydrophilic coating before bonding. The capillary transport mechanism in nonwoven wicking geotextiles results from the interaction between the material's porous fibrous network and a proprietary hydrophilic treatment applied to the fibers. The surface treatment converts the naturally hydrophobic fibers into hydrophilic ones and promotes rapid wetting and efficient water transport without compromising the lateral drainage characteristics of conventional nonwoven geotextiles (Liu et al., 2025b).

The reference NG material contains untreated hydrophobic polyester filaments and therefore serves as a baseline for highlighting the effectiveness of the surface treatments. According to information provided by the manufacturer, WGv2 received a greater treatment dosage than WGv1. The coating chemistry and dosage are proprietary and were not independently quantified in this study. Both wicking products form the textile component of wicking geocomposite systems, in which a biaxial polypropylene geogrid is thermally bonded to the nonwoven geotextile to combine mechanical reinforcement with moisture control. The present investigation, however, isolated the geotextile layer since it alone dictates liquid transport. Table 1 presents the mechanical and hydraulic properties of the three geotextiles, as obtained from manufacturer specifications and third-party laboratory measurements.

Water, glycerin, and mineral oil were selected as wetting liquids for the droplet contact angle tests because they represent a broad range of surface tension, polarity, and viscosity. This selection allows for a comprehensive assessment of how interfacial tensions and viscous resistance influence capillary flow through the porous structure of the nonwoven fabrics. The properties of the test liquids are summarized in Table 2.

As shown in Table 2, water and glycerin are both polar liquids with similar surface tensions but markedly different viscosities, with glycerin exhibiting a viscosity approximately 740 times greater than that of water. This large difference in viscosity allowed glycerin to be used as a probe liquid for investigating droplet spreading and imbibition on the wicking geotextiles, where water absorption occurred too rapidly to be accurately recorded and interpreted because of transient dynamic effects. Consequently, glycerin provides a slowed-down representation of

Table 2
Properties of the probe liquids.

Test Liquid	Density	Surface Tension	Kinematic viscosity	Polarity
	g/ml	N/m	centi Stokes	-
Water	1.00	0.072	1	Polar
Glycerin	1.24	0.069	740	Polar
Mineral Oil	0.85	0.030	65	Non-polar

Table 1
Mechanical and hydraulic parameters of the nonwoven geotextiles.

Geotextile	Property	Unit	Value	Standard	Image
WGv_1	AOS	Microns	75	ASTM D 4751	
	Permittivity	l/s	1.55	ASTM D 4491	
	Flow rate	$l/min/m^2$	4717	ASTM D 4491	
	Unit mass	g/m^2	255	ASTM D 5261	
	Filament Density	dtex	4	ISO 1973	
	Thickness	mm	1.67	ASTM D5199	
	Grab tensile strength	N	1087	ASTM D 4632	
	Grab elongation	%	85	ASTM D 4632	
	Trapezoid tear	N	485	ASTM D 4533	
WGv_2	AOS	Microns	75	ASTM D 4751	
	Permittivity	l/s	1.54	ASTM D 4491	
	Flow rate	$l/min/m^2$	4689	ASTM D 4491	
	Unit mass	g/m^2	249	ASTM D 5261	
	Filament Density	dtex	5.2	ISO 1973	
	Thickness	mm	1.57	ASTM D5199	
	Grab tensile strength	N	1092	ASTM D 4632	
	Grab elongation	%	86	ASTM D 4632	
	Trapezoid tear	N	482	ASTM D 4533	
NG	AOS	Microns	75	ASTM D 4751	
	Permittivity	l/s	1.64	ASTM D 4491	
	Flow rate	$l/min/m^2$	4247	ASTM D 4491	
	Unit mass	g/m^2	242	ASTM D 5261	
	Thickness	mm	1.94	ASTM D5199	
	Grab tensile strength	N	971	ASTM D 4632	
	Grab elongation	%	71	ASTM D 4632	
	Trapezoid tear	N	365	ASTM D 4533	

the wetting and imbibition processes that occur with water, enabling the rapid hydraulic interactions between water and the geotextile to be more readily observed and interpreted. Also, mineral oil, a nonpolar liquid with substantially lower surface tension, was employed to investigate the influence of wettability on wickability. Owing to the polarity compatibility between mineral oil and polyester fibers, together with its low surface tension, mineral oil exhibited a wetting regime on all tested geotextiles, providing additional insight into the contribution of wettability in capillary transport.

2.2. Filtration-induced clogging in the WGv$_2$ sample

A laboratory filtration experiment was performed to induce glass bead impregnation within the geotextile and to examine the consequent change in hydraulic response. The use of spherical soda lime glass beads instead of natural soil particles eliminates the variability in shape, surface chemistry, and mineral composition commonly encountered with natural soils. The use of glass beads as a surrogate for natural soil particles in investigations of geotextile clogging has been adopted in previous studies (Palmeira et al., 2005; Palmeira and Trejos Galvis, 2016). Nevertheless, glass beads do not reproduce the angularity, mineralogical heterogeneity, surface roughness, plasticity, organic content, or physicochemical interactions of embankment soils. Therefore, the results should be interpreted as a controlled and accelerated assessment of the hydraulic effects of particle impregnation rather than as a direct simulation of a specific field soil or aggregate.

A circular specimen of WGv2, 150 mm in diameter, was placed on a porous support, and a 300-mm-high column of glass beads was carefully packed above the fabric inside an acrylic tube to simulate an overlying soil layer [Fig. 1(a)]. The glass bead mixture was prepared at an initial gravimetric water content of 15% and placed into the acrylic test column in six successive layers, each approximately 50 mm thick and compacted with a total compaction energy of 15.9 kJ/m^3.

After saturating and deairing the system, water was introduced from the top under a constant hydraulic gradient of four. The constant hydraulic head was maintained throughout the filtration test using a constant head filtration system consisting of a water supply reservoir connected to a circulation pump, an inlet pressure reservoir, and a back-pressure reservoir. The circulation pump continuously supplied water to the system, while the inlet and back-pressure reservoirs maintained a constant head difference across the specimen. In addition, an inline particle filter was installed in the recirculation loop to prevent migrated glass beads from being reintroduced into the system. The flow was maintained for roughly 5 h, even though flow rate measurements indicated that most fine particle migration and clogging took place within the first few minutes, as shown in Fig. 1(b).

A relatively high hydraulic gradient of four, which is uncommon under field conditions, was intentionally selected to accelerate particle migration and induce an extreme filtration-induced clogging condition within a practical laboratory timescale. This procedure was designed to produce a partially clogged condition through accelerated particle impregnation, providing material-scale insight into one possible degradation mechanism. Although most particle migration occurred during the initial stage of the test because of the internally unstable particle size distribution, filtration was continued until the flow rate stabilized.

The particle size distribution of the glass beads was purposely configured to be internally unstable, as illustrated in Fig. 1(c). This distribution, which possesses a concave upward gradation curve and a high uniformity coefficient, produces a gap-graded distribution in which the fine fraction (10 percent by mass, passing sieve No. 200) can move through the voids between coarse particles, a process known as suffusion (Palmeira, 2025). As migration progressed, fine particles accumulated both on the surface and within the matrix of the geotextile, reducing the permeability of the developing filter cake until steady conditions were achieved. Upon completion of the test, the geotextile was carefully extracted, and residual beads were removed from its surface. The retention capacity of the partially clogged specimen was then measured, revealing a considerable reduction in void volume, as summarized in Table 3. Microscopic images captured before and after the test, presented in Fig. 2(a) and (b), respectively, clearly display the entrapment of glass beads within the particle-impregnated geotextile structure.

Microscopic images were acquired at multiple randomly selected locations across each specimen to account for the inherent heterogeneity of the nonwoven fiber network, including variations in fiber spacing, orientation, and local particle distribution. The images presented in Fig. 2 are representative of the pore morphology and fiber arrangement

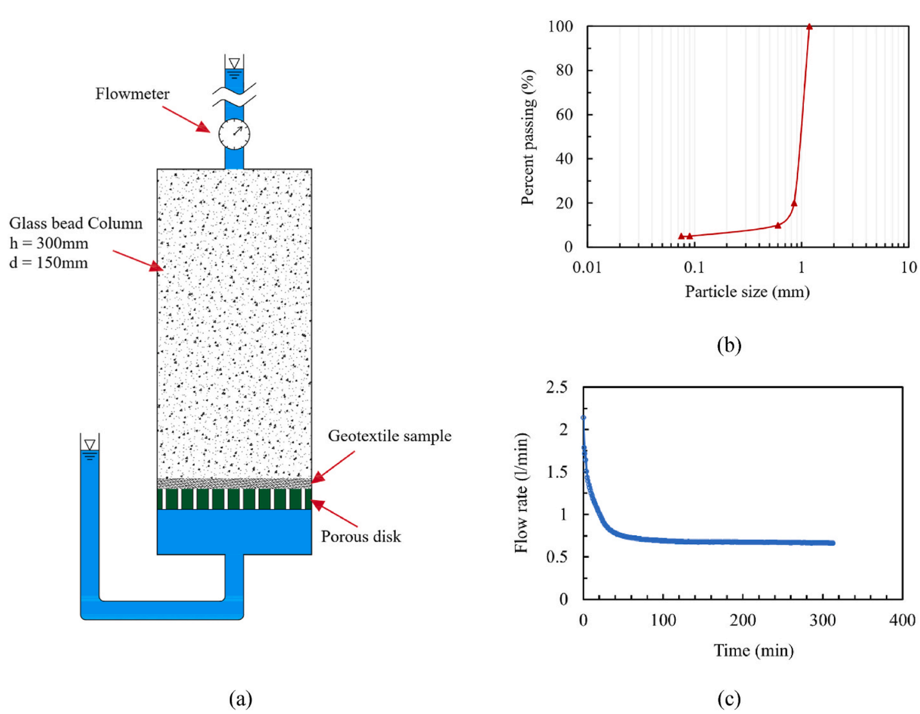

Fig. 1. Filtration experiment: (a) setup; (b) particle size distribution; (c) flow rate change.

Table 3
Gravimetric liquid content (ω) of virgin and particle-impregnated geotextile specimens.

Geotextile	ω (water)	ω (mineral oil)
NG	8.87	12.56
WGv_1	6.89	9.92
WGv_2	6.2	9.10
WGv_2 *(Clogged)*	4.7	7.3

$\omega = w_L/w_{dry}$; where w_L is the mass of liquid saturating the sample, w_{dry} is the mass of the dry sample.

observed across the specimens and are intended only as qualitative illustrations of particle impregnation within the fibrous structure.

3. Results and discussion

As previously mentioned, wicking refers to the spontaneous movement of liquid within a porous medium driven by capillary forces arising from surface wetting. Wicking was defined by Kissa (1996) as spontaneous wetting and is mathematically described, for idealized parallel capillaries, by the Lucas–Washburn equation (Washburn, 1921). This equation (Eq. (1)) is extensively employed to calculate the unidirectional wicking rate or the advancement distance of the wetting front, which is driven by capillary pressure gradients in interconnected porous media (Ansari and Haghighat Kish, 2000; Sharabaty et al., 2008). The driving capillary pressure is expressed by Eq. (2), representing the pressure difference (ΔP) across the curved liquid–vapor interface as derived from Laplace's law.

$$\frac{dL}{dt} = \frac{r\gamma \cos\theta}{4\eta L} \quad (1)$$

$$\Delta P = \frac{2\gamma}{r}\cos\theta \quad (2)$$

$$\gamma_{SV} - \gamma_{SL} = \gamma_{VL}\cos\theta \quad (3)$$

In these equations, L denotes the wicking length, γ represents the surface tension at the liquid–vapor interface, η indicates the viscosity of the liquid, θ is the intrinsic contact angle between the solid and the liquid, and r signifies the capillary radius. These relationships underscore that wicking rate and capillary pressure are inherently functions of both pore size and wettability. Surface tension in this context refers to the vapor–liquid (*VL*) interfacial tension, which, in equilibrium with the solid–liquid (*SL*) and solid–vapor (*SV*) interfacial tensions, determines the contact angle as described by Young's equation (Eq. (3)). Another key factor, indirectly represented in Young's equation, is the polarity of the solid and liquid phases, which affects interfacial tensions and governs wetting behavior. A match in polarity between the liquid and solid tends to enhance the wetting regime, whereas a mismatch can adversely affect it (Ahmad et al., 2018; Wu, 1973). Polyester is inherently nonpolar, while the surface treatment applied to the wicking geotextile fibers increases their polarity. This modification imparts hydrophilic characteristics to the treated fibers, enabling them to absorb polar liquids such as water. The polarity classifications of the test liquids used in this study are summarized in Table 2.

According to Eq. (2), in wetting regimes, characterized by contact angles ranging from 0° to 90°, capillary pressure remains positive, enabling capillary-driven fluid flow. Moreover, the Lucas-Washburn equation shows an increase in the wicking rate with pore size, while Eq. (2) indicates that capillary pressure decreases with increasing pore size. This occurs because viscous friction, governed by Poiseuille's law, serves as the primary resistance within the Lucas-Washburn framework. Larger pores, despite having lower capillary pressure, facilitate higher flow rates due to reduced viscous resistance.

The Lucas–Washburn equation was originally developed to describe

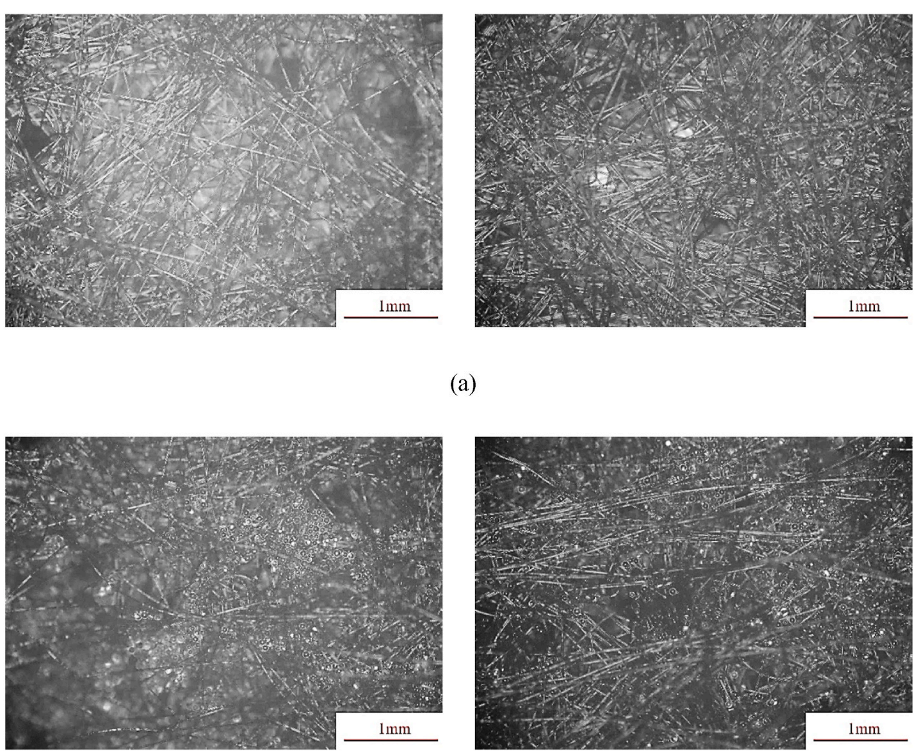

(b)

Fig. 2. Microscopic images of (a) virgin WGv_2 and (b) impregnated WGv_2 samples.

one-dimensional capillary flow in parallel capillary tubes under the assumption of negligible gravitational effects. Chen et al. (2001) and Sharabaty et al. (2008) demonstrated the applicability of the Lucas-Washburn equation in predicting the wicking rate in yarns and woven fabrics. However, water transport mechanisms differ in nonwoven geotextiles, where fluid flow occurs through the complex, interconnected spaces between randomly oriented fibers. Equivalent capillary tube models must therefore incorporate additional variables to represent such media accurately (Rengasamy, 2006). Key structural parameters, including fiber orientation and diameter, porosity, pore size distribution, capillary space geometry, and continuity and length of water pathways, can influence capillary flow and therefore need to be evaluated for accurate estimation of wicking rate in nonwoven fibers (Mao and Russell, 2008). In this study, the Lucas–Washburn equation was used only to provide a qualitative interpretation of the observed wicking behavior and to compare trends under different wetting regimes and wettability conditions. The simplified form presented in Eq. (1) was not intended to provide accurate quantitative predictions for the nonwoven fibrous structures.

A series of experiments was conducted in this study to evaluate the wickability of nonwoven geotextiles by examining their interactions with water, glycerin, and mineral oil as the testing liquids. The use of these liquids across the three geotextile types introduced a broad spectrum of wettability conditions and pore structures. Investigating and comparing these combinations clarifies the distinction between wettability and wickability and enhances the understanding of moisture transport mechanisms in nonwoven geotextiles.

3.1. Contact angle measurement

The contact angle between a liquid and a solid (θ) results from the equilibrium among solid–liquid, solid–vapor, and liquid–vapor interfacial tensions, a relationship described by Young's equation (Eq. (3)). A lower contact angle (CA) signifies a greater degree of wettability, which reflects either a higher surface energy of the solid or a lower surface energy of the liquid, both of which facilitate the advancement of the liquid over the surface. In wicking geotextiles, enhancing the solid surface energy through a polar hydrophilic fiber coating reduces the contact angle and improves wettability for polar liquids such as water. Rengasamy (2006) drew on Young's equation to define wetting regimes as those where the contact angle lies between 0° and 90°, and non-wetting regimes where the angle ranges from 90° to 180°. Kutilek and Nielsen (1994) classified wetting behaviour into complete wetting ($\theta = 0$), incomplete wetting ($0 < \theta < 90°$), and non-wetting ($\theta \geq 90°$) regimes.

The intrinsic contact angle is a fundamental measure of a material's wettability. Although it can be measured on smooth, ideal surfaces using liquid droplet tests, direct measurement of this property in porous media is impractical under both wetting and nonwetting conditions. In wetting regimes, droplets placed on fibrous substrates are unstable and undergo imbibition, causing the contact angle to continuously decrease. In such cases, the contact angle is often approximated as zero, as is done in porometry analyses using the capillary flow test, where the intrinsic contact angle is treated as an input parameter (Elton and Hayes, 2008). In nonwetting conditions, despite remaining on the surface of the porous medium without deformation, the droplet interacts with both solid fibres and air, and therefore does not represent the intrinsic contact angle of the solid (Frank and Perré, 2012).

In this study, the contact angle and the evolution of liquid droplets were measured using a custom-built goniometer setup developed in the Surface Engineering Laboratory at McGill University. As depicted in Fig. 3, the apparatus consists of a high-speed camera (HSC) operating at 30 frames per second and a computer-controlled syringe pump to ensure consistent and precise droplet deposition. Shadowgraphic videos were captured and analyzed frame-by-frame using image processing software to calculate the contact angle and droplet geometry based on the double-sided elliptical fitting method (Asadi et al., 2022). This method, applied to detect the contact point and determine the contact angle, has been shown to yield stable and accurate measurements with minimal error due to distortions (Andersen and Taboryski, 2017). To minimize interference from the wavy structure of the nonwoven substrate and ensure accurate identification of the droplet base, droplets were deposited at the apex of a gently curved section. In the liquid droplet method, the contact angle is defined as the internal angle formed between the tangent to the liquid–vapor interface and the solid surface at the three-phase contact line, as illustrated in Fig. 4.

3.1.1. Liquid droplets on nonwicking geotextile

Fig. 5 shows that water and glycerin droplets of varying sizes placed on the NG sample remain on the surface without changes in contact angle, contact radius, height, and volume due to the non-wetting regime between these liquids and the nonwicking geotextile. The contact angle measurement was performed after the droplet reached equilibrium, following the dissipation of inertial energy that initially caused droplet vibration upon placement on the surface. From Fig. 5, it can be inferred that the intrinsic contact angle between the solid component of NG and the liquids (water and glycerin) is more than 90° but the exact intrinsic value cannot be determined as the droplet is in contact with both solid

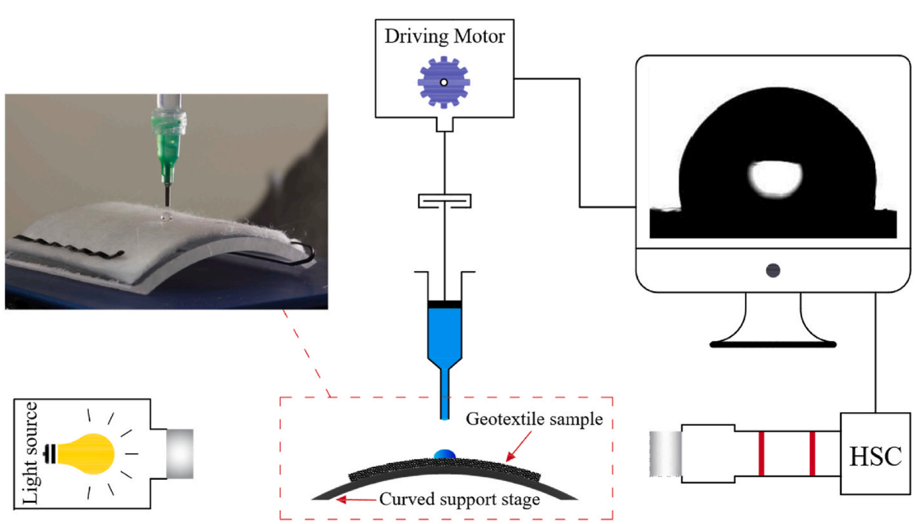

Fig. 3. Goniometer setup for contact angle experiment.

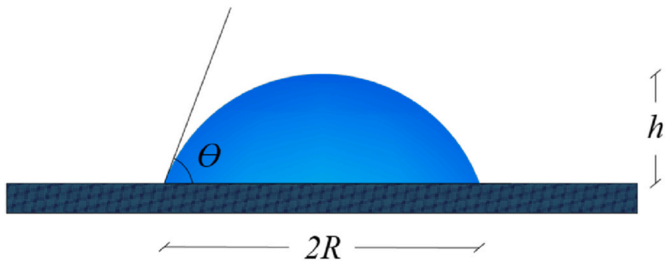

Fig. 4. Parameters measured during liquid droplet analysis.

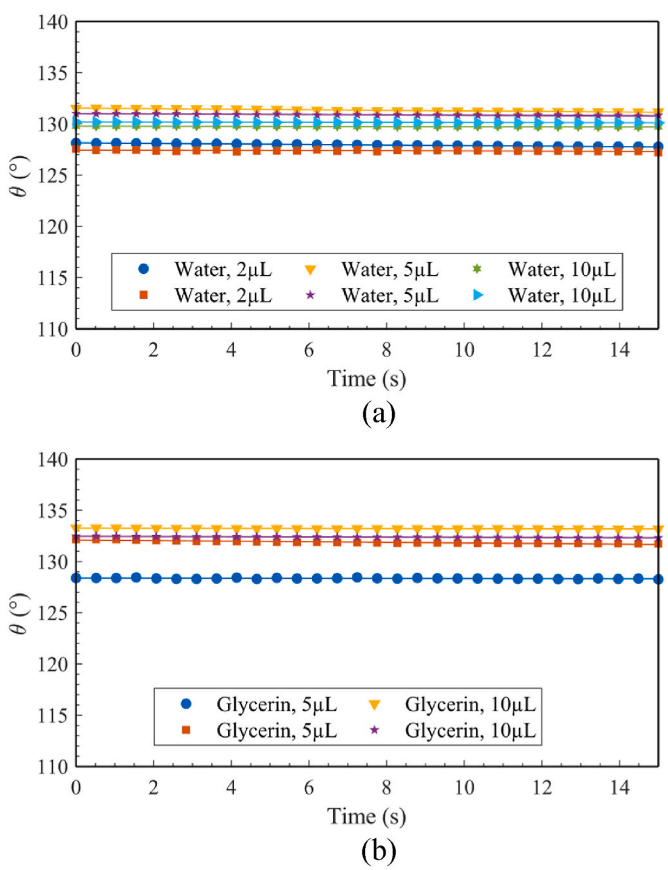

Fig. 5. Contact angle variation with time on NG sample: (a) water droplet; (b) glycerin droplet.

and air and the apparent contact angle is a function of pore size, surface pore density, and roughness (Cassie and Baxter, 1944; Denesuk et al., 1994; Frank and Perré, 2012).

It can also be observed that for small droplet sizes used in this study (2 to 10 μl), where the gravity effect is negligible, droplet volume has no influence on contact angle (Liu et al., 2025b; Zaman et al., 2022). The reason for the large range of the recorded contact angle from different tests is attributed to the random structure of the nonwoven geotextiles. Additionally, the identical average apparent contact angles measured for glycerin and water are attributed to their closely matched surface tension and polarity.

According to Young's equation, liquid–solid interactions are governed by the equilibrium of surface energies. Given that mineral oil has a substantially lower vapor–liquid interfacial tension than both water and glycerin, the placement of a mineral oil droplet on the nonwicking geotextile induces a wetting response. Moreover, the non-polar nature of both mineral oil and polyester reinforces this wetting behavior due to the inherent affinity between non-polar materials (Ahmad et al., 2018). As shown in Fig. 6(a), an 8 μL droplet of mineral oil was fully absorbed within 0.3 s, despite its kinematic viscosity being approximately 65 times greater than that of water. The sequential absorption process is also depicted in Fig. 6(b). These observations demonstrate that in the presence of a suitable pore structure, a wetting regime can initiate capillary flow.

3.1.2. Mineral oil droplet on geotextile samples

The time-dependent spreading and imbibition of a liquid droplet on a porous medium are controlled by the interplay of capillary pressure, curvature-driven gradients, gravity force, and viscous resistance (Frank and Perré, 2012; Sarah and Ulrich, 2018). Fig. 7 andFig. 8 summarize the interaction of an 8-μL mineral oil droplet with the three nonwoven geotextiles examined in this study, showing the evolution of contact angle, droplet height, contact radius, and imbibed volume over time. The spreading and imbibition behavior of the droplets on the tested samples is consistent with patterns reported in the literature for liquid–solid interactions on porous substrates under wetting regimes (Clarke et al., 2002; Kumar and Deshpande, 2006).

In these figures, contact radius, droplet height, and imbibed volume are presented in dimensionless form as R/R_{max}, h/h_0, and V_{imb}/V_0 where R, R_{max}, h, h_0, V_{imb}, and V_0 represent the contact radius, maximum contact radius, droplet height, initial droplet height, imbibed volume, and initial droplet volume, respectively. The parameter t_{max} denotes the time required for complete droplet absorption. The imbibed volume was calculated for each frame based on the geometry of a spherical cap, assuming a circular base and symmetric profile, using geometric relations described in Equations (4) and (5) (Meric and Erbil, 1998).

$$V = \frac{\pi h}{6}\left(3R^2 + h^2\right) \tag{4}$$

$$V_{imb} = V_0 - V \tag{5}$$

The spreading and imbibition of a liquid droplet can be divided into discrete stages characterised by the temporal evolution of contact radius (Kumar and Deshpande, 2006; Zhdanov et al., 2003). Fig. 7(c) illustrates the three well known stages of droplet evolution under wetting conditions, where capillary action drives liquid imbibition into the porous structure while the droplet simultaneously spreads across the surface. In the initial stage, driven by Laplace pressure, the base radius expands over time, following a power law until it reaches its maximum value (Tanner, 1979). During this phase, the contact angle and droplet height decrease more rapidly than in the subsequent stages, while viscous resistance gradually overcomes inertial effects (Biance et al., 2004). The second stage is defined by a period during which the contact radius remains nearly constant. In the final stage, the contact radius begins to shrink, driven by capillary forces, ultimately leading to complete droplet absorption.

Fig. 8(b) presents the variation of imbibed droplet volume as a function of the square root of time. Excluding the initial and final data points, a clear linear trend is observed during the intermediate stage. This linear behavior is consistent with the findings of Kumar and Deshpande (2006), who reported similar trends during the second stage of droplet evolution for silicone oil and polyvinyl alcohol water solutions on glass fiber mats. A comparable pattern was also discussed by Denesuk et al. (1993) during the second phase of droplet evolution on a porous substrate in a wetting regime.

More notably, in Fig. 8(a), the rate of mineral oil imbibition, which reflects the wicking rate of the geotextile samples for this liquid, is more than twice as high in the nonwicking sample. WGv_1 also exhibits a slightly higher wicking rate than WGv_2. To explain these trends, it is important to first consider the polarity compatibility between the nonwicking sample and mineral oil, which enhances wetting behavior, as discussed in section 3.1.1. Additionally, consider the Lucas-Washburn equation, which, as previously discussed, indicates a direct

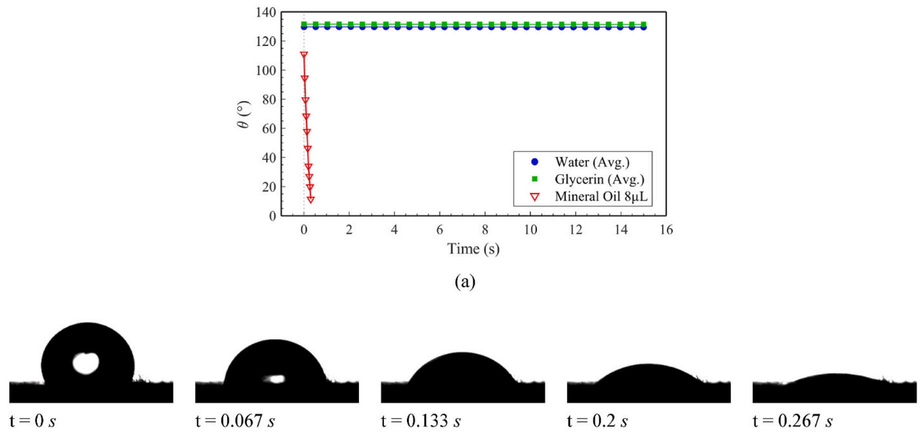

Fig. 6. Droplet analysis on NG sample: (a) contact angle variation over time, (b) sequential images of mineral oil droplet spreading and imbibition.

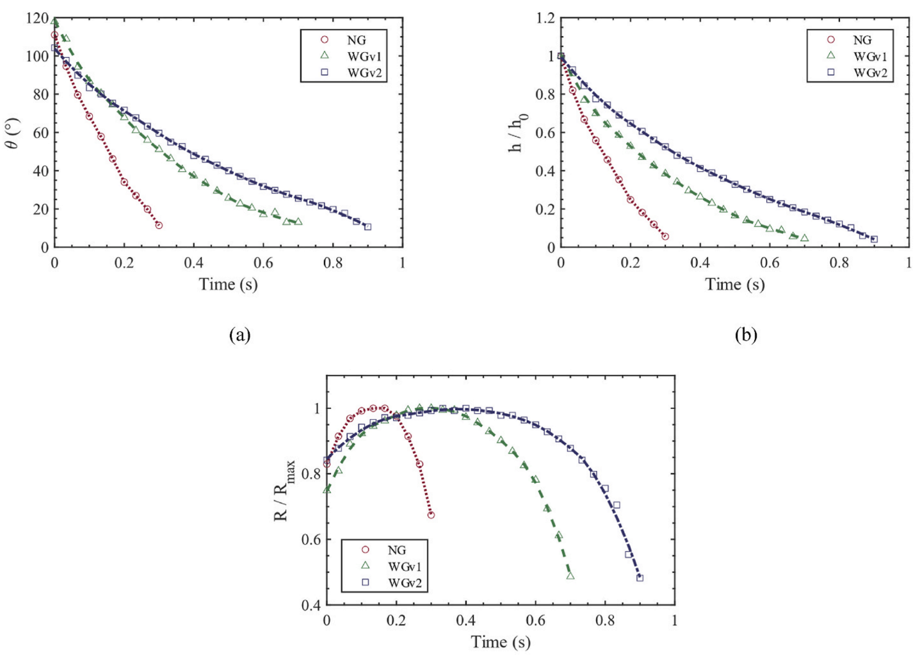

Fig. 7. Temporal evolution of mineral oil droplet on nonwoven geotextiles: (a) apparent contact angle, (b) normalized droplet height, and (c) normalized contact radius, all measured over time.

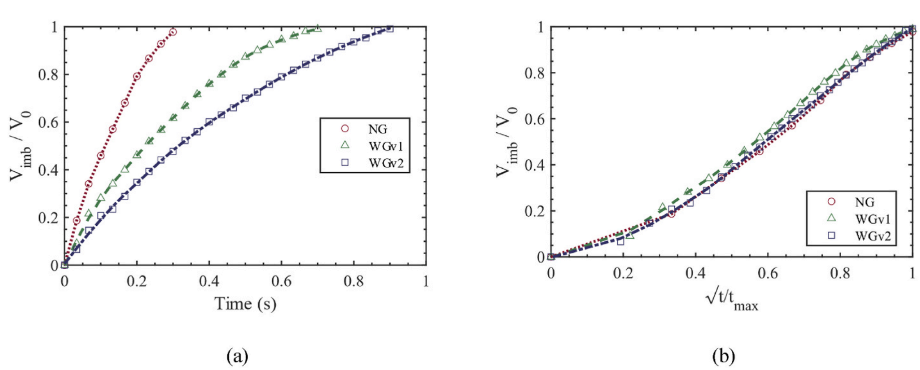

Fig. 8. Variation of imbibed volume of a mineral oil droplet with (a) time and (b) the square root of normalized time.

relationship between wicking rate and pore size. Although the Apparent Opening Size values reported in Table 1 are the same for all three geotextiles, this measurement reflects only the O_{95} value, which corresponds to the pore diameter below which ninety-five percent of the pores fall. Moreover, this value was determined using the dry glass bead sieving method according to ASTM-D4751, and was reported as the nearest standard sieve size. Consequently, AOS cannot adequately characterize or distinguish differences in the pore structure of the investigated geotextiles.

Capillary flow porometry (ASTM-D6767) was performed on the three geotextiles to characterize their pore-size distribution. The porometry curves exhibited a systematic shift among the materials, suggesting a progressively denser pore network from NG to WGv1 and WGv2. However, because capillary flow porometry is influenced by the liquid–solid contact angle (Elton and Hayes, 2008), obtaining accurate pore characteristics for geotextiles with different surface energies requires further investigation.

To characterize the internal structure of the geotextiles, gravitational liquid retention values are presented in Table 3. These results, along with the nearly identical mass per unit area values reported in Table 1, indicate that the fully saturated nonwicking sample retains a significantly larger volume of liquid. This observation suggests a higher volume of accessible pores in the NG structure than in the wicking geotextiles. WGv1 also retains slightly more liquid than WGv2, which may explain its marginally higher wicking performance (Table 4), assuming comparable inherent wettability between mineral oil and both wicking fibers. In fact, the lower porosity of the wicking samples, particularly WGv2, increases viscous resistance to fluid flow, further reducing the wicking rate. This interpretation will be further examined in the following section by analyzing glycerin droplets, given their polarity compatibility with the hydrophilic coating applied to the wicking samples. Ezzatneshan and Goharimehr (2020) similarly reported lower droplet imbibition rates in compact fibrous media compared to those with more open fiber arrangements.

3.1.3. Glycerin and mineral oil droplets on wicking geotextiles

A series of experiments was conducted by placing 8-μL glycerin droplets on the surface of the wicking geotextiles. The results were compared with those obtained using mineral oil, as shown in Fig. 9. A similar test could not be performed with water droplets on the wicking samples because water was absorbed too rapidly to be accurately recorded and analyzed, and it could not be stabilized on the surface of the fibers during placement. This immediate absorption behavior of water on nonwoven wicking fibers was also observed and reported by Liu et al. (2025b). Glycerin is a polar liquid, similar to water, with a surface tension comparable to that of water but a viscosity approximately 740 times higher, which prolongs the imbibition process and allows for detailed analysis. A higher imbibition rate was observed for mineral oil droplets compared to glycerin in Fig. 9(c), on both wicking samples. This is attributed to the lower surface tension and viscosity of mineral oil, despite its polarity incompatibility with the hydrophilic coating on the wicking fibers, which weakens the wetting regime.

According to the data presented in Fig. 9(c), WGv_1 consistently exhibited a higher wicking rate than WGv_2 for both test liquids (see Table 4). However, the difference in performance was more pronounced for glycerin, underscoring the critical influence of pore structure on capillary flow. This suggested that the viscous resistance was sufficiently high that glycerin's polar compatibility with the hydrophilic coating on the wicking fibers could not compensate for the reduction in wicking rate. It also highlights the importance of clearly distinguishing between the terms "wettability" and "wickability", which are often used interchangeably in geotechnical applications.

Moreover, due to the lower glycerin imbibition rate on the WGv_2 sample, the transition between spreading phases is more clearly visible in Fig. 9(a) and (b). As discussed earlier, the most rapid decline in contact angle occurs during the first stage, when the contact area expands to its maximum value. A change in the rate of contact angle reduction was observed in Fig. 9(a) as the process transitioned from the second to the third phase, during which the droplet began to shrink until it was fully absorbed.

3.1.4. Influence of clogging on spreading and imbibition dynamics

The long-term hydraulic and mechanical performance of nonwoven geotextiles can be affected by particle impregnation during soil placement and compaction, or by the migration of fine particles into the geotextile matrix under fluid flow (Chen et al., 2008; Palmeira, 2025; Palmeira and Fannin, 2002; Palmeira and Gardoni, 2000, 2002; Rollin and Lombard, 1988). While the effects of clogging were extensively studied in the context of saturated hydraulic properties, few investigations addressed its influence on capillary flow in wicking fibers (Lin et al., 2017). Palmeira and Fannin (2002) evaluated the reduction in porosity caused by particle accumulation within the nonwoven geotextile structure and reported changes spanning several orders of magnitude. This highlights the potential role of particle impregnation in influencing capillary flow, given the critical role of porosity.

In this study, contact angle tests were performed on dried WGv_2 samples that had been impregnated with glass beads finer than Sieve No. 200 during the filtration experiment as described in section 2.2. Eight-microliter droplets of mineral oil and glycerin were placed on the sample surfaces, and their spreading and imbibition dynamics were compared with those observed on virgin WGv_2 samples. The test results, summarized in Fig. 10 and Fig. 11, revealed contrasting trends for the two liquids. For mineral oil, a comparison of pre- and post-clogging behavior showed a marked increase in wicking rate, with droplet absorption occurring approximately 2.5 times faster on the clogged WGv_2 sample. In contrast, glycerin droplets exhibited a substantial reduction in wicking rate, requiring nearly 4 times longer to be fully absorbed on the clogged surface (see Table 4).

The enhanced wicking rate observed for mineral oil may be attributed to partial alteration or removal of the polar hydrophilic coating due to prolonged water flow during the clogging procedure. This reduced the sample's polarity and strengthened the wetting interaction between mineral oil and the clogged wicking sample, despite the porosity reduction caused by particle impregnation.

Fig. 10(c) depicts the stepwise evolution of the glycerin droplet, characterized by noticeable lags during which the droplet radius remained constant for extended periods. This behavior can be explained by the fact that, in wetting porous media, the fluid front within the material advances ahead of the visible superficial spreading front of the droplet (Clarke et al., 2002; Davis and Hocking, 2000; Kumar and

Table 4
Summary of the liquid transport performance of the investigated geotextiles.

Geotextile	Wicking rate (μL/s)			Interpretation
	Water[a]	Glycerin[b]	Mineral oil[b]	
NG	No absorption	No absorption	1.95	Hydrophobicity suppresses polar-liquid absorption.
WGv1	300	0.29	1.63	29%, 47%, and 136% higher wicking rates than WGv2 for water, glycerin, and mineral oil, respectively.
WGv2	233	0.20	0.69	Reduced porosity constrained capillary liquid transport
WGv2 (Clogged)	133	0.03	1.68	43% and 83% reductions in water and glycerin transport, but a 143% increase in mineral-oil transport.

[a] Values were obtained from the horizontal wicking test under **continuous liquid supply**.
[b] Values were obtained from 8-μL droplet tests (**finite liquid volume**).

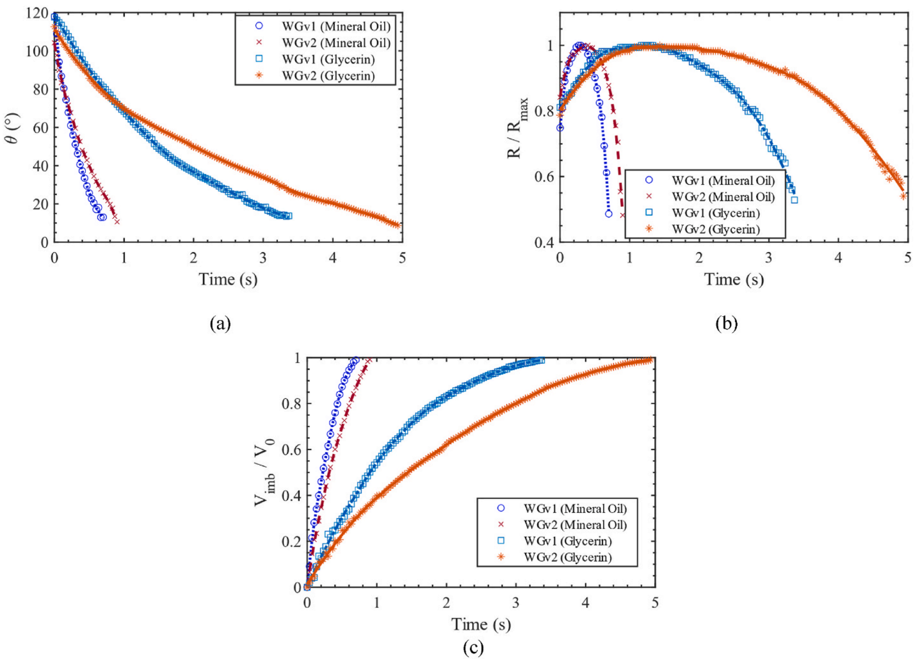

Fig. 9. Time-dependent behavior of glycerin and mineral oil droplets on wicking geotextile: (a) apparent contact angle, (b) normalized contact radius, and (c) normalized imbibed volume.

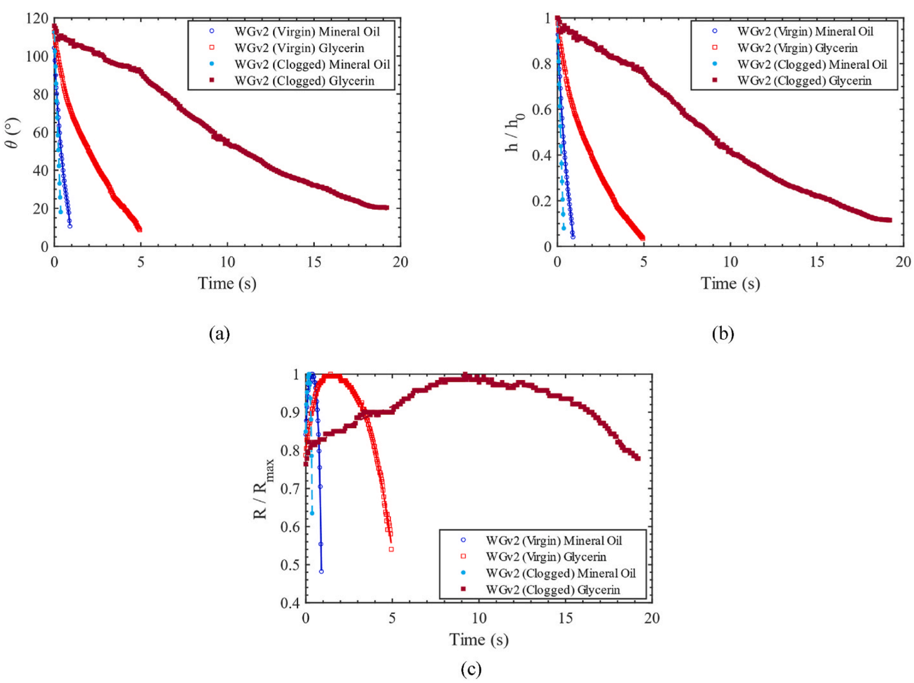

Fig. 10. Evolution of glycerin and mineral oil droplets on the clogged WGv2 surface: (a) apparent contact angle, (b) normalized droplet height, and (c) normalized contact radius, plotted over time.

Deshpande, 2006). In clogged samples, reduced porosity and the high viscous resistance of glycerin in regions with significant clogging caused the internal fluid front to slow down or temporarily halt. This resulted in a delayed or stalled droplet spread, a phenomenon that has also been reported by Ezzatneshan and Goharimehr (2020) in numerical simulations of droplet spreading on compact fibrous media compared to more porous configurations.

Furthermore, as mentioned above, fluid flow during the filtration process partially rinsed off the hydrophilic coating and weakened the wettability regime between glycerin and wicking fibers. This change adversely affected the wicking rate of glycerin, which is a polar liquid. Although available evidence suggests that both particle impregnation and partial coating removal influence wettability, further research is needed to quantify the contribution of each factor. Successful efforts have been made by the manufacturer to enhance the durability of the hydrophilic coating applied to wicking fibers in harsh environmental conditions.

Furthermore, the linear relationship between imbibed volume and the square root of time, which typically characterizes the second stage of droplet evolution, did not persist in the clogged samples, particularly for

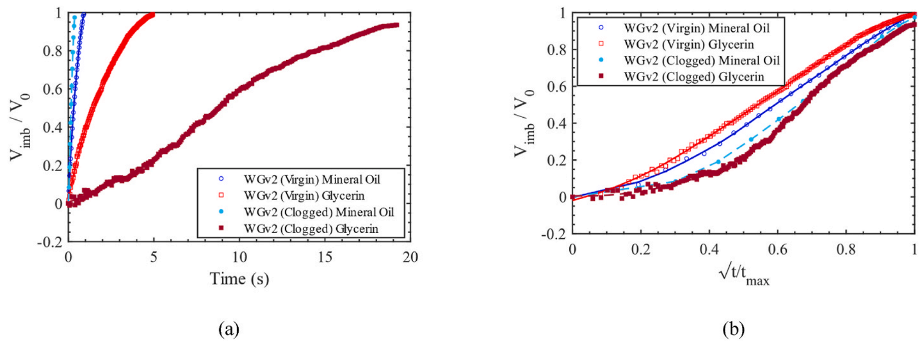

Fig. 11. Imbibed volume of glycerin and mineral oil droplets on the clogged WGv_2 sample versus (a) time and (b) $\sqrt{(t/t_{max})}$.

glycerin droplets. This deviation can be attributed to reduced porosity, increased tortuosity, and heterogeneity in the distribution of glass beads within the geotextile structure. Tan (2022) also reported a similar deviation in this relationship, attributing it to changes in the droplet-to-pore size ratio, which in turn alter the imbibition dynamics.

Droplet imbibition tests were performed ten times for each liquid–geotextile combination. The curve presented in the manuscript corresponds to one of the repeated tests and was selected as a representative example of the observed imbibition behavior. The reported imbibition rates shown in Fig. 12 were calculated by averaging all imbibition rate measurements. The mean imbibition rates and the corresponding standard deviations are summarized in Fig. 12.

3.2. Horizontal radial wicking from an infinite water source

Wicking experiments are typically categorized into those involving wicking from an infinite liquid reservoir and those involving wicking from a finite liquid reservoir (Kissa, 1996; Patnaik et al., 2006; Rengasamy, 2006). This distinction is important, as the wicking behavior can be influenced by the volume of available liquid. Xiao et al. (2012) reported a linear relationship between absorption volume and time for infinite reservoir conditions, whereas nonlinear behavior has been observed in finite-volume conditions (Kissa, 1996; Middleman, 1998; Tan, 2022).

The droplet spreading and absorption behavior described earlier represents a typical case of wicking from a finite liquid volume. Although field conditions are influenced by transient hydraulic events, such as intermittent rainfall, groundwater fluctuations, and unsaturated water redistribution, wicking geotextiles typically require hours to days to remove excess moisture and restore the surrounding soil to its pre-event moisture state. During this period, the surrounding soil acts as a relatively large, although finite, moisture reservoir. Consequently, the infinite liquid supply test provides a more representative laboratory boundary condition for evaluating sustained capillary transport than droplet absorption, which represents only a transient wetting event. Nevertheless, the horizontal infinite liquid supply wicking test remains an idealized laboratory configuration and does not fully reproduce the hydraulic boundary conditions encountered in the field.

As demonstrated in Figs. 8(a)–9(c) and 11(a), these experiments showed a nonlinear relationship between imbibed volume and time during droplet evolution. However, in practical field applications, wicking geotextiles function under conditions more akin to an infinite liquid supply. Additionally, as discussed above, droplet analyses could not be performed with water on the surface of the wicking geotextiles due to the extremely rapid absorption rate, even though these geotextiles are primarily intended to drain water in field applications. Moreover, droplet-based analyses may be influenced by the nonhomogeneous structure of the geotextile, as the localized area involved in spreading and absorption during contact angle measurements may not accurately represent the overall material behavior.

To address these limitations, the wicking rates of WGv_1, WGv_2, and clogged WGv_2 were measured using an infinite water source, based on the method proposed by Van Der Meeren et al. (2002) with minor modifications. The test setup is illustrated in Fig. 13. In this experiment, a water meniscus comes into contact with the center of a 100-mm diameter geotextile disk, whose edge is secured within a suspended

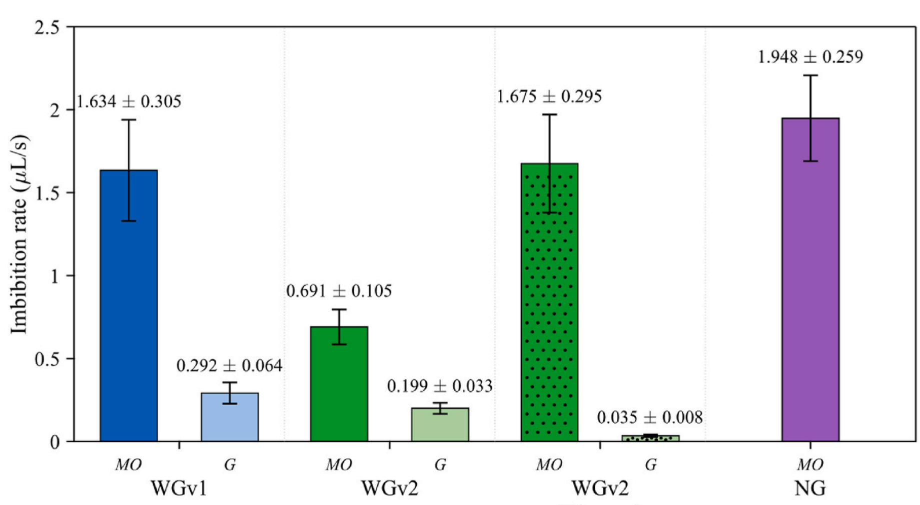

Fig. 12. Comparison of the imbibition rates of 8 μL mineral oil (MO) and glycerin (G) droplets on WGv1, WGv2, clogged WGv2, and non-wicking geotextile (NG). Error bars represent standard deviation (n = 10).

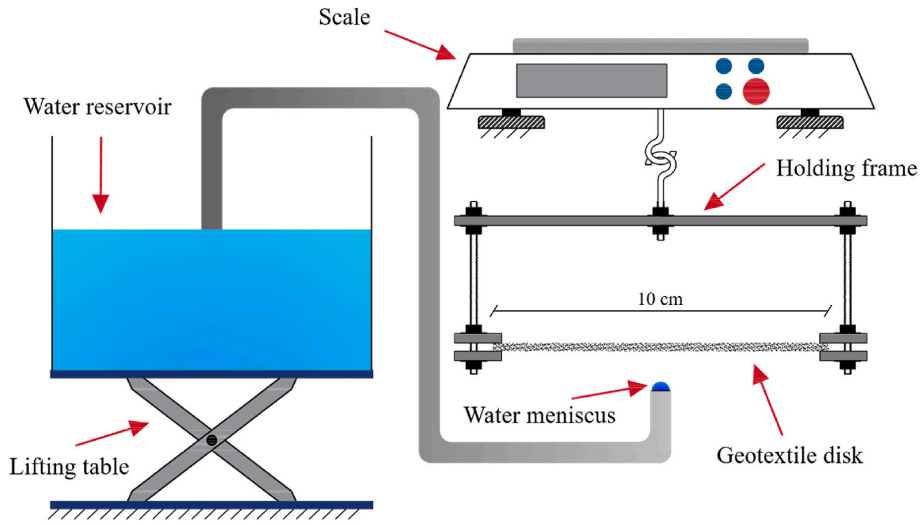

Fig. 13. Experimental setup for measuring horizontal wicking from an infinite water reservoir.

frame attached to a scale with 0.01-g resolution. As soon as the meniscus touches the sample, capillary flow initiates radially within the wicking geotextiles. The scale records the increase in weight over time, corresponding to water absorption, until full saturation is reached.

A specimen diameter of 100 mm was selected to provide sufficient radial distance for capillary transport while minimizing potential boundary effects. In addition, because needle-punched nonwoven geotextiles exhibit local variations in fiber orientation and pore structure, a 100 mm specimen was considered sufficiently large to provide a representative characterization of the material microstructure. The liquid reservoir was positioned at the center of the specimen to produce symmetric radial imbibition. Because the imbibition rate was determined before the wetting front reached the specimen boundary, edge effects on the measured wicking rate were considered negligible.

As shown in Fig. 14, water initially wicked into the geotextile at a constant rate, producing a linear increase in absorbed mass. The slope of this curve represents the wicking rate. WGv1 and WGv2 exhibited mean wicking rates of 18 ± 1.05 and 14 ± 1.80 g/min (mean ± standard deviation), respectively. The horizontal radial wicking test was repeated three times for each geotextile, as indicated in Fig. 14. Absorption ceased once the samples became fully saturated. The higher wicking rate of WGv1 can be attributed to its greater porosity, which reduces viscous resistance, despite the low viscosity of water. Fig. 15 shows the results for the clogged WGv2 sample, where a substantial decline in wicking rate was observed. The data followed a nonlinear trend, with full saturation reached in approximately 100 s and an average wicking rate of 8 g/min. The clogged WGv2 specimen did not exhibit a distinct initial linear stage in Fig. 15 from which a representative wicking rate could be determined. This behavior is due to particle impregnation, which altered the pore structure and capillary flow paths, causing the wetting front to advance irregularly rather than as a symmetric radial front. Consequently, the wicking rate was calculated as the average absorption rate by dividing the total absorbed water by the corresponding test duration.

The marked decline in wicking performance of the clogged sample (Table 4) is attributed to the combined effects of reduced porosity and diminished wettability. The weight and packing of the glass bead column, together with particle impregnation, reduced geotextile porosity and thereby increased viscous resistance. Additionally, the leaching of hydrophilic treatment agents during prolonged water filtration reduced wettability, which in turn lowered the wicking rate in this case.

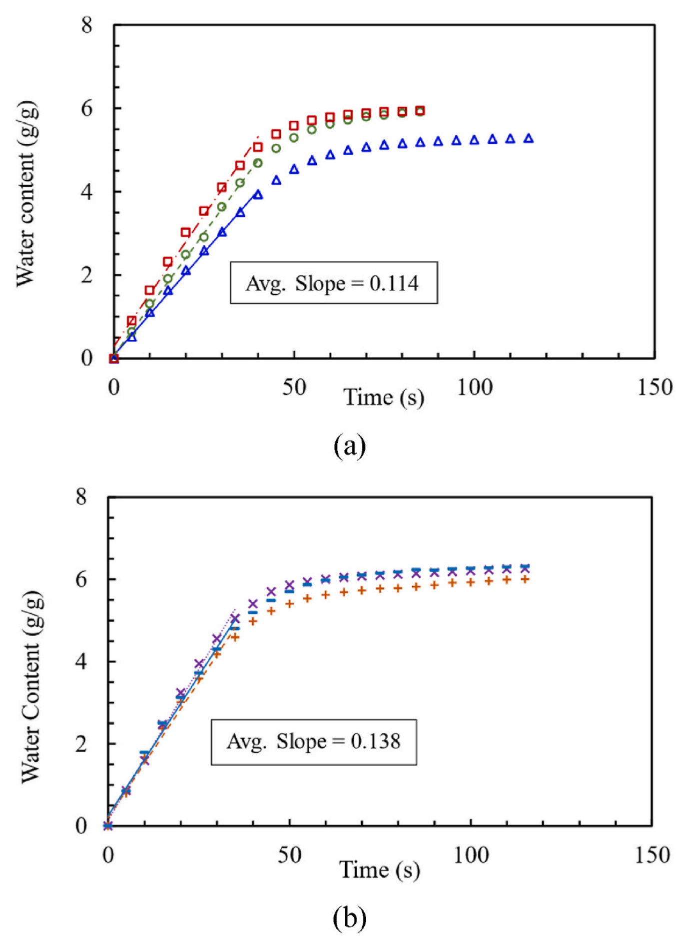

Fig. 14. Variation of gravitational water content over time: (a) WGv_2 sample; (b) WGv_1 sample.

4. Conclusion

While wicking has been extensively studied in the textile literature as capillary flow in fibrous media, geotechnical engineering has traditionally relied on principles of unsaturated soil mechanics to describe wettability and wickability of geotextiles. However, conventional testing methods and interpretative frameworks used in soil mechanics are not fully suited for the hydraulic characterization of wicking geotextiles, particularly when distinguishing between wetting and wicking

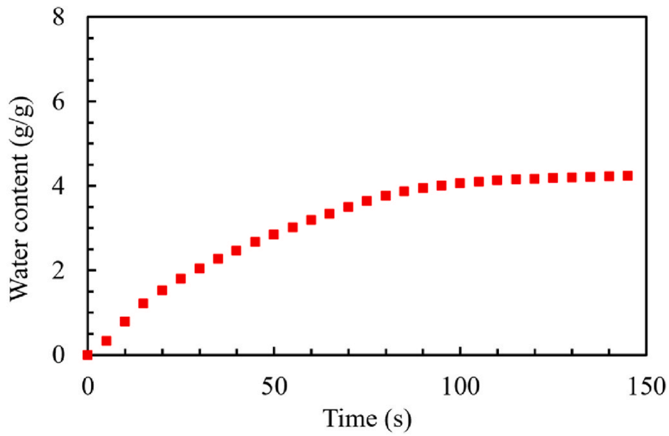

Fig. 15. Gravitational water content change over time for the clogged WGv_2 sample.

phenomena. To address this interdisciplinary gap, this study adopted testing approaches from textile and surface engineering research to better characterize the capillary behavior of wicking geotextiles. The wickability of two nonwoven wicking geotextiles (WGv_1 and WGv_2) and their nonwicking counterpart (NG) was evaluated through contact angle measurements with various liquids and an infinite-reservoir radial wicking test using water. The objective was to clarify and differentiate the concepts of wettability and wickability, emphasizing the critical role of pore structure in governing capillary flow in nonwoven geotextiles. These insights contribute to more informed material selection based on field-specific conditions.

The adopted laboratory testing methods were designed to isolate the fundamental mechanisms governing moisture transport in nonwoven wicking geotextiles under well-controlled conditions. The droplet imbibition and horizontal wicking tests characterize the intrinsic effects of wettability and pore structure on liquid transport. Also, the filtration process was designed to simulate particle accumulation within the geotextile resulting from field dynamics such as seepage-driven fine migration. In transportation embankments, cyclic traffic loading and repeated seepage events can induce the migration of fine particles toward the geotextile, where they may accumulate within the fibrous pore network over time and progressively alter its hydraulic characteristics. The accelerated filtration-induced clogging test provides preliminary insight into one aspect of the hydraulic performance deterioration in nonwoven wicking geotextiles.

To achieve a representative clogged state within a practical laboratory timescale, particle migration was accelerated by applying a relatively high hydraulic gradient. The adopted procedure provides a controlled and comparative assessment of the influence of filtration-induced clogging on hydraulic performance, rather than a direct simulation of the complete long-term field aging process, which may also involve repeated wetting–drying cycles, traffic loading, and environmental degradation. Comprehensive assessment of long-term field performance also requires consideration of repeated freeze-thaw cycles, traffic-induced deformation, environmental aging, and site-specific hydraulic conditions, which are beyond the scope of this study.

Liquid droplet analysis on the nonwicking (NG) sample revealed resistance to water and glycerin penetration due to its low surface energy and polarity mismatch. In contrast, the rapid absorption of mineral oil illustrates a favorable wetting regime, driven by the compatibility of surface energies and non-polar interactions between the liquid and the polyester fibers. Meanwhile, both wicking geotextiles absorbed all test liquids, with WGv1 consistently exhibiting higher wicking rates than WGv2, despite WGv2's additional treatment. This trend is attributed to WGv1's more open structure and aligns with the qualitative relationship between pore size and wicking rate described by the Lucas–Washburn equation. In the clogged WGv2 sample, partial removal of the hydrophilic treatment likely reduced the surface polarity and increased the affinity for mineral oil, resulting in a 140% increase in its wicking rate. In contrast, the wicking rates of glycerin and water decreased by approximately 80% and 40%, respectively, due to reduced wettability and decreased pore volume.

It is worth noting that selecting an optimal wicking geotextile should not rely solely on the wicking rate. The combination of greater treatment dosage and a denser fiber structure in WGv2 may result in higher capillary suction than in WGv1, potentially promoting greater moisture uptake from adjacent unsaturated soil under high suction conditions despite its lower intrinsic wicking rate. Moreover, the geotextile's pore structure should be carefully matched to the gradation of the surrounding soil to mitigate clogging risks and ensure sustained long-term hydraulic performance.

Finally, this study provides a material-scale evaluation of the influence of wettability, pore structure, and filtration-induced clogging on the wicking behavior of nonwoven geotextiles. Although these properties are fundamental to field performance, the hydraulic response of wicking geotextiles in service is also governed by factors such as soil type, suction conditions, hydraulic boundary conditions, confinement, and drainage outlet conditions. Therefore, the laboratory results presented herein should be interpreted as material-scale characteristics rather than direct predictors of field-scale drainage performance.

CRediT authorship contribution statement

Ali Pezeshki: Conceptualization, Data curation, Formal analysis, Investigation, Methodology, Writing – original draft. **Mohamed A. Meguid:** Project administration, Supervision, Validation, Writing – review & editing. **Sam Bhat:** Funding acquisition, Writing – review & editing.

Declaration of competing interest

The authors declare the following financial interests/personal relationships which may be considered as potential competing interests: Given Professor Mohamed Meguid's role as associate editor, he had no involvement in the peer review of this article and had no access to information regarding its peer review. Full responsibility for the editorial process for this article was delegated to another journal editor. If there are other authors, they declare that they have no known competing financial interests or personal relationships that could have appeared to influence the work reported in this paper.

Acknowledgments

This work was supported by an NSERC Alliance Grant co-funded by Titan Environmental Containment Ltd. The authors acknowledge Titan for supplying the geotextile samples and providing valuable technical support throughout the project.

Data availability

Data will be made available on request.

References

Ahmad, D., Van Den Boogaert, I., Miller, J., Presswell, R., Jouhara, H., 2018. Hydrophilic and hydrophobic materials and their applications. Energy Sources, Part A Recovery, Util. Environ. Eff. 40, 2686–2725.
Andersen, N.K., Taboryski, R., 2017. Drop shape analysis for determination of dynamic contact angles by double sided elliptical fitting method. Meas. Sci. Technol. 28, 047003.
Ansari, N., Haghighat Kish, M., 2000. The wicking of water in yarn as measured by an electrical resistance technique. J. Textil. Inst. 91, 410–419.

Asadi, M.B., Aboud, D.G., Wood, M.J., Zeppetelli, G., Kietzig, A.-M., 2022. A new insight into dynamic contact angle measurements: implementation of smooth splines method. Colloids Surf. A Physicochem. Eng. Asp. 655, 130234.
ASTM-D4751, 2012. Standard Test Method for Determining Apparent Opening Size of a Geotextile. American Society for Testing and Materials, Philadelphia, PA, USA.
ASTM-D6767, 2014. Standard Test Method for Pore Size Characteristics of Geotextiles by Capillary Flow Test. American Society for Testing and Materials.
Aydilek, A.H., D Hondt, D., Holtz, R.D., 2007. Comparative evaluation of geotextile pore sizes using bubble point test and image analysis. Geotech. Test. J. 30, 173–181.
Azevedo, M., Zornberg, J., 2013. Capillary barrier dissipation by new wicking geotextile. In: al, C.e. (Ed.), Panamerican Conference on Unsaturated Soils. Taylor & Francis Group, Cartagena de Indias, Colombia, pp. 559–565.
Bai, Y., Yang, W., Shi, B., Liu, L., Wang, M., Wang, S., Song, X., Tian, C., 2024. Optimization design and analysis of irregular cross-sectional structure in water conducting fibers. Geotech. Geol. Eng. 42, 6147–6164.
Biance, A.-L., Clanet, C., Quéré, D., 2004. First steps in the spreading of a liquid droplet. Phys. Rev. 69, 016301.
Bouazza, A., 2014. A simple method to assess the wettability of nonwoven geotextiles. Geotext. Geomembranes 42, 417–419.
Bouazza, A., Zornberg, J.G., McCartney, J.S., Nahlawi, H., 2006. Significance of unsaturated behaviour of geotextiles in earthen structures. Aust. Geomech. 41, 133–142.
Bouazza, A., Zornberg, J.G., McCartney, J.S., Singh, R.M., 2013. Unsaturated geotechnics applied to geoenvironmental engineering problems involving geosynthetics. Eng. Geol. 165, 143–153.
Brooks, R., Corey, A., 1965. Hydraulic Properties of Porous Media, Civil Engineering Department. Colorado State University, Fort Collins.
Cassie, A., Baxter, S., 1944. Wettability of porous surfaces. Trans. Faraday Soc. 40, 546–551.
Chen, R.-H., Ho, C.-C., Chung, W.-B., 2008. The filtration mechanism and micro-observation of soil-geotextile systems under cyclic flows. J. GeoEng. 3, 101–112.
Chen, X., Kornev, K.G., Kamath, Y.K., Neimark, A.V., 2001. The wicking kinetics of liquid droplets into yarns. Textil. Res. J. 71, 862–869.
Clarke, A., Blake, T., Carruthers, K., Woodward, A., 2002. Spreading and imbibition of liquid droplets on porous surfaces. Langmuir 18, 2980–2984.
Davis, S.H., Hocking, L.M., 2000. Spreading and imbibition of viscous liquid on a porous base. II. Phys. Fluids 12, 1646–1655.
Denesuk, M., Smith, G., Zelinski, B., Kreidl, N., Uhlmann, D.R., 1993. Capillary penetration of liquid droplets into porous materials. J. Colloid Interface Sci. 158, 114–120.
Denesuk, M., Zelinski, B., Kreidl, N., Uhlmann, D., 1994. Dynamics of incomplete wetting on porous materials. J. Colloid Interface Sci. 168, 142–151.
Elton, D., Hayes, D., 2008. The significance of the contact angle in characterising the pore size distribution of geotextiles. Geosynth. Int. 15, 22–30.
Ezzatneshan, E., Goharimehr, R., 2020. Study of spontaneous mobility and imbibition of a liquid droplet in contact with fibrous porous media considering wettability effects. Phys. Fluids 32.
Frank, X., Perré, P., 2012. Droplet spreading on a porous surface: a lattice Boltzmann study. Phys. Fluids 24, 042101.
Galinmoghadam, J., Liu, J., Zhang, X., Lin, C., Guo, Y., 2022. Mitigating pumping in pavement shoulder using wicking geotextile: an experimental study. Transp. Res. Rec. 2676, 145–159.
Guo, Y., Zou, D., Hu, M., Zhang, X., Xu, F., Zhang, Y., Chen, J., 2026. Influence of wicking geotextile installation on moisture migration in silt under rainfall infiltration. Geotext. Geomembranes 54, 25–35.
Han, J., 2015. Principles and Practice of Ground Improvement. John Wiley & Sons, Hoboken, NJ, USA.
Harnett, P., Mehta, P., 1984. A survey and comparison of laboratory test methods for measuring wicking. Textil. Res. J. 54, 471–478.
Haynes, J., Yoder, E., 1963. Effects of repeated loading on gravel and crushed stone base course materials used in the AASHO road test. Joint Highway Research Project, Indiana Department of Transportation and Purdue University, Lafayette.
Jarjour, J., Meguid, M., Bhat, S., 2024. Water retention characterization of non-woven geotextiles: an application for wicking materials. GeoAmericas 2024. EDP Sciences.
Kim, J.-H., Kwon, D.-J., Lim, C.-S., Seo, B.-K., DeVries, K.L., Park, J.-M., 2022. Interfacial adhesion evaluation via wettability for fiber reinforced polymer composites: a review. Compos. Interfaces 30, 283–299.
Kissa, E., 1996. Wetting and wicking. Textil. Res. J. 66, 660–668.
Koerner, R.M., 2012. Designing with Geosynthetics-, vol. 1. Xlibris Corporation, p. 6.
Kumar, S.M., Deshpande, A.P., 2006. Dynamics of drop spreading on fibrous porous media. Colloids Surf. A Physicochem. Eng. Asp. 277, 157–163.
Kutilek, M., Nielsen, D.R., 1994. Soil Hydrology. Catena-Verlag. Cremlingen-Destedt.
Lekarp, F., Isacsson, U., Dawson, A., 2000. State of the art. II: permanent strain response of unbound aggregates. J. Transport. Eng. 126, 76–83.
Li, L., Liu, J., Zhang, X., Saboundjian, S., 2011. Resilient modulus characterization of Alaska granular base materials. Transport. Res. Board 2232, 44–54.
Lin, C., Presler, W., Zhang, X., Jones, D., Odgers, B., 2017. Long-term performance of wicking fabric in Alaskan pavements. J. Perform. Constr. Facil. 31, D4016005.
Lin, C., Zhang, X., Galinmoghadam, J., Guo, Y., 2022. Working mechanism of a new wicking geotextile in roadway applications: a numerical study. Geotext. Geomembranes 50, 323–336.
Lin, C., Zhang, X., Han, J., 2016. Development of a Design Method for H2Ri Wicking Fabric in Pavement Structures.
Lin, C., Zhang, X., Han, J., 2018. Comprehensive material characterizations of pavement structure installed with wicking fabrics. J. Mater. Civ. Eng. 31, 04018372.
Liu, M., Liu, J., Bhat, S., Gao, Y., Lin, C., 2025a. Model tests on wicking geosynthetic composite reinforced bases over weak subgrade. Geotext. Geomembranes 53, 938–949.
Liu, M., Liu, J., Bhat, S., Gupta, R., Lin, C., 2025b. Evaluation of water removal capability of wicking nonwoven geotextiles. Geotext. Geomembranes 53, 1228–1241.
Ma, C., Feng, H., Wang, C., Zhang, N., Liu, Y., Li, J., Liu, X., Li, S., Jiang, H., Li, Y., 2024. A numerical simulation of moisture reduction in fine soil subgrade with wicking geotextiles. Materials 17, 390.
Mao, N., Russell, S.J., 2008. Capillary pressure and liquid wicking in three-dimensional nonwoven materials. J. Appl. Phys. 104, 034911.
Meric, R.A., Erbil, H.Y., 1998. Evaporation of sessile drops on solid surfaces: pseudospherical cap geometry. Langmuir 14, 1915–1920.
Middleman, S., 1998. An Introduction to Fluid Dynamics : Principles of Analysis and Design. Wiley, New York.
Palmeira, E., 2025. Geotextile filters: from idealization to real behaviour (Giroud Lecture 2023). Geosynth. Int. 32, 2–39.
Palmeira, E., Gardoni, M., Bessa da Luz, D., 2005. Soil–geotextile filter interaction under high stress levels in the gradient ratio test. Geosynth. Int. 12, 162–175.
Palmeira, E., Fannin, R., 2002. Soil-geotextile compatibility in filtration. Proceedings 7th International Conference on Geosynthetics, pp. 853–870.
Palmeira, E., Gardoni, M., 2000. The influence of partial clogging and pressure on the behaviour of geotextiles in drainage systems. Geosynth. Int. 7, 403–431.
Palmeira, E., Gardoni, M., 2002. Drainage and filtration properties of non-woven geotextiles under confinement using different experimental techniques. Geotext. Geomembranes 20, 97–115.
Palmeira, E.M., Trejos Galvis, H.L., 2016. Opening sizes and filtration behaviour of nonwoven geotextiles under confined and partial clogging conditions. Geosynth. Int. 24, 125–138.
Patnaik, A., Rengasamy, R., Kothari, V., Ghosh, A., 2006. Wetting and wicking in fibrous materials. Textil. Prog. 38, 1–105.
Rengasamy, R.S., 2006. Wetting phenomena in fibrous materials. In: Pan, N., Gibson, P. (Eds.), Thermal and Moisture Transport in Fibrous Materials. Woodhead Publishing Series in Textiles, pp. 156–187.
Rollin, A., Lombard, G., 1988. Mechanisms affecting long-term filtration behavior of geotextiles. Geotext. Geomembranes 7, 119–145.
Sarah, K., Ulrich, H., 2018. Short timescale wetting and penetration on porous sheets measured with ultrasound, direct absorption and contact angle. RSC Adv. 8, 12861–12869.
Sharabaty, T., Biguenet, F., Dupuis, D., Viallier, P., 2008. Investigation on moisture transport through polyester/cotton fabrics. Indian J. Fibre Text. Res. 33, 419–425.
Stormont, J.C., Morris, C.E., 2000. Characterization of unsaturated nonwoven geotextiles. Advances in Unsaturated Geotechnics, pp. 153–164.
Sylvestre, O., Bilodeau, J.-P., Doré, G., 2019. Effect of frost heave on long-term roughness deterioration of flexible pavement structures. Int. J. Pavement Eng. 20, 704–713.
Tan, H., 2022. Absorption of millimeter-and micrometer-sized droplets on nylon powder. Exp. Fluid 63, 187.
Tanner, L.H., 1979. The spreading of silicone oil drops on horizontal surfaces. J. Phys. Appl. Phys. 12, 1473–1484.
Uzan, J., 2004. Permanent deformation in flexible pavements. J. Transport. Eng. 130, 6–13.
Van Der Meeren, P., Cocquyt, J., Flores, S., Demeyere, H., Declercq, M., 2002. Quantifying wetting and wicking phenomena in cotton terry as affected by fabric conditioner treatment. Textil. Res. J. 72, 423–428.
Van Genuchten, M.T., 1980. A closed-form equation for predicting the hydraulic conductivity of unsaturated soils. Soil Sci. Soc. Am. J. 44, 892–898.
Washburn, E.W., 1921. The dynamics of capillary flow. Phys. Rev. 17, 273–283.
Wu, S., 1973. Polar and nonpolar interactions in adhesion. J. Adhes. 5, 39–55.
Xiao, J., Stone, H.A., Attinger, D., 2012. Source-like solution for radial imbibition into a homogeneous semi-infinite porous medium. Langmuir 28, 4208–4212.
Zaman, M.W., Han, J., Zhang, X., 2022. Evaluating wettability of geotextiles with contact angles. Geotext. Geomembranes 50, 825–833.
Zhang, X., Presler, W., Li, L., Jones, D., Odgers, B., 2014. Use of wicking fabric to help prevent frost boils in Alaskan pavements. J. Mater. Civ. Eng. 26, 728–740.
Zhdanov, S., Starov, V., Sobolev, V., Velarde, M., 2003. Spreading of aqueous SDS solutions over nitrocellulose membranes. J. Colloid Interface Sci. 264, 481–489.
Zhong, W., 2006. Surface tension, wetting and wicking. Thermal and Moisture Transport in Fibrous Materials. Woodhead Publishing Series in Textiles, pp. 136–155.
Zornberg, J., Bouazza, A., McCartney, J., 2010. Geosynthetic capillary barriers: current state of knowledge. Geosynth. Int. 17, 273–300.
Zornberg, J.G., Azevedo, M., Sikkema, M., Odgers, B., 2017. Geosynthetics with enhanced lateral drainage capabilities in roadway systems. Transp. Geotechn. 12, 85–100.